WindSat Wind Vector Retrievals without Explicit Atmospheric Modeling

Emre Ertin, *Member, IEEE,* Joel T. Johnson, *Senior Member, IEEE*

***Abstract*— We present a probabilistic model and an associated wind vector retrieval algorithm for WindSat polarimetric radiometer measurements. The model describes measured brightnesses in a given frequency channel and polarization as a function of the wind speed and direction only; other effects, including atmospheric and other sea surface contributions, are not parametrized explicitly, but rather modeled as correlated random disturbances on brightness azimuthal harmonic coefficients. The probabilistic model leads to a simple maximum likelihood estimator for wind speed and direction, and the performance of this estimator is examined using matchups between WindSat and QuikScat data. Despite the probabilistic modeling of atmospheric and non-wind related sea-surface contributions, the estimator's performance is comparable to the performance achieved in other WindSat wind vector retrievals, including the EDR 1.8.1 product. The method's performance is studied further through the use of analytical estimates of retrieval performance for other radiometer channel configurations.**

***Index Terms*— Microwave Radiometry, Ocean Wind Vector Estimation**

I. Introduction

MEasurements of global wind vectors provide important information for weather forecasts and scientific studies in oceanography and climatology. Interest in using microwave radiometers for ocean wind vector measurements has increased in the past decade, because recent studies have shown that the addition of polarimetric channels can enhance wind direction retrieval performance. WindSat is the first spaceborne polarimetric microwave radiometer, and provides fully polarimetric measurements in three frequency bands as well as dual polarized measurements in two other frequencies [1]; the WindSat dataset represents the first large-scale opportunity for the wind vector retrieval performance achievable by a polarimetric radiometer to be assessed. Wind vector retrievals from WindSat data have been examined in several previous studies [2].

A key issue for retrievals of wind direction involves the variation of observed brightnesses with the relative azimuthal angle between the radiometer look direction and the wind direction. Previous studies have shown that these dependencies can be expressed in a set of sine- and cosine-functions in the relative azimuth angle, with linearly polarized brightnesses consisting of cosine functions, while the polarimetric channels are sine-functions. Therefore the linearly polarized and polarimetric channels provide complementary wind direction signatures, so that use of both, if possible, is likely to yield enhanced wind direction retrievals. The overall amplitude of brightness variations with wind direction is typically around 1 K or less, so that accurate brightness measurements are required to observe these variations.

Use of the linearly polarized channels for wind direction retrievals is complicated by the strong influence of the atmosphere as well as other environmental parameters on these channels. For example, at 18.7 GHz, the sensitivity of the horizontally polarized brightness to columnar integrated water vapor is roughly one K brightness per one mm of integrated water vapor. Because this sensitivity to a relatively small change in integrated water vapor is comparable to the maximum variation with wind direction, it is very difficult to separate atmospheric variations from wind direction effects. While retrievals of wind direction have been performed using only the linearly polarized channels [3], the wind direction retrievals produced required a high degree of spatial and temporal averaging in order to provide sufficient reduction of atmospheric variations.

Atmospheric effects are greatly reduced in the polarimetric channels because these channels involve differences between brightnesses in two polarizations; because atmospheric contributions are largely unpolarized, the differencing procedure largely eliminates them. However, atmospheric attenuation as well as the reflection of downwelling atmospheric brightness from the sea surface remain in the polarimetric channels. A simple algorithm representing these contributions in terms of a "transmissivity squared" has been derived and used in previous studies [4].

Although several investigations of wind vector retrievals from WindSat have utilized the polarimetric channels only in wind direction retrievals because of these facts, the WindSat environmental data record (EDR) version 1.8.1 produced by the Naval Research Laboratory [5]-[6] uses a physically-based retrieval algorithm that includes all channels in the wind direction retrieval. In particular, a model for atmospheric effects on all channels is included in the retrieval, so that there is some possibility that the wind direction retrieval can make use of information from the linearly polarized channels. However the degree to which wind direction retrievals are benefited by inclusion of the linearly polarized channels has not been quantified.

In this paper, the performance of an alternative retrieval approach that neglects any explicit modeling of atmospheric effects is investigated. The goal of the study is to compare the algorithm's performance with that achieved by WindSat EDR 1.8.1, in order to provide information on the degree to which EDR 1.8.1's attempts to explicitly model atmospheric effects

Manuscript received Month dd, yyyy; revised Month dd, yyyy. This work was supported by the National Polar-Orbiting Operational Environmental Satellite System Integrated Program Office and by the Naval Research Laboratory

E. Ertin and J. T. Johnson are with The Ohio State University, Department of Electrical and Computer Engineering.

are benefiting wind direction retrievals. It will be shown that the proposed algorithm achieves an overall retrieval performance that is comparable to that of the WindSat EDR 1.8.1, suggesting that the methods used for removing atmospheric effects in EDR 1.8.1 are providing only marginal gains in wind vector retrieval performance. Note that the current WindSat EDR 1.9.0 product was not available at the time the studies of this paper were performed, and improvements in wind vector retrieval performance for EDR 1.9.0 compared to EDR 1.8.1 have been reported [6]; future work will extend this comparison to include EDR 1.9.0.

The proposed algorithm is based on a simple probabilistic model that describes observed brightness azimuthal harmonic coefficients as a multi-variate Gaussian random vector, with the mean vector and covariance matrix of the random vector modeled only as a function of wind speed. We present a method for estimating the mean and covariance of the harmonic coefficients directly from brightness temperature data, perform maximum likelihood retrievals for a subset of WindSat observations, and compare the wind vectors retrieved from WindSat with those from EDR 1.8.1 and from collocated QuikScat scatterometer wind vector retrievals. In addition, it is straight forward to derive an analytical estimate of retrieval performance under this model; these estimates are used to demonstrate that retrieval performance under this model depends strongly on both wind speed and wind direction.

The rest of the paper is organized as follows. In Section II we present the multivariate Gaussian model of WindSat data, relate it to a parametric model of harmonic coefficients, and derive the associated maximum likelihood estimator (MLE) of wind speed and direction. Section III discusses estimation of model parameters from collocated WindSat and QuikScat [6] measurements. In Section IV we illustrate the performance of the maximum likelihood estimator for WindSat measurements using empirical retrieval studies and comparisons with QuikSCAT wind retrievals as well as WindSat EDR 1.8.1. A discussion of the algorithm's implicit operations that reduce atmospheric effects is provided in Section V. Analytical prediction of MLE estimator performance is then discussed in Section VI, with results from these predictions provided in Section VII. Section VIII concludes with remarks for future research.

II. A Probabilistic Model for WindSat data

WindSat polarimetric brightness temperatures are described in terms of vertically and horizontally polarized brightnesses (T_v and T_h) and their cross-correlations (T_U and T_V) given by:

$$\begin{bmatrix} T_v \\ T_h \\ T_U \\ T_V \end{bmatrix} = \begin{bmatrix} < E_v E_v^* > \\ < E_h E_h^* > \\ 2\mathrm{Re} < E_v E_h^* > \\ 2\mathrm{Im} < E_v E_h^* > \end{bmatrix} \tag{1}$$

where E_v and E_h represent values proportional to the time harmonic electric fields measured by the radiometer in vertical and horizontal polarizations, respectively. These four polarimetric channels are sensitive to ϕ, the relative azimuthal angle between the wind direction and the radiometer look direction.

An analysis [7] of scattering by reflection symmetric media shows that T_v and T_h are even functions of ϕ, whereas T_U and T_V are odd functions of ϕ. A truncated Fourier series expansion of these functions yields a model for the four polarimetric channels parametrized in terms of the relative wind direction as:

$$\begin{aligned} T_v &= T_{v0}(W) + T_{v1}(W)\cos(\phi) + T_{v2}(W)\cos(2\phi) \\ T_h &= T_{h0}(W) + T_{h1}(W)\cos(\phi) + T_{h2}(W)\cos(2\phi) \\ T_U &= T_{U1}(W)\sin(\phi) + T_{U2}(W)\sin(2\phi) \\ T_V &= T_{V1}(W)\sin(\phi) + T_{V2}(W)\sin(2\phi) \end{aligned} \tag{2}$$

The harmonic coefficients (i.e. T_{v0}, T_{v1}, etc.) depend in general on incidence angle, frequency, wind-speed W, and other atmospheric and surface properties, but are modeled as functions of the windspeed only.

The WindSat radiometer measures brightnesses in five frequency bands: $6.8, 10.7, 18.7, 23.8$ and 37.0 GHz. The $10.7, 18.7$ and 37.0 GHz channels are fully polarimetric, while the 6.8 and 23.8 GHz channels measure only T_v and T_h. A single WindSat measurement thus contains 16 brightness temperatures:

$$\mathbf{T} = [T_v^1, T_h^1, T_v^2, \ldots, T_v^5, T_h^5, T_U^5, T_V^5]^T \tag{3}$$

where the superscript T indicates the transpose operator, and the numeric superscripts serve as indices to to the five WindSat frequency channels in order of increasing frequency. The second order harmonic model for WindSat measurements can now be written as:

$$\mathbf{T} = \mathbf{B}(\phi)\mathbf{H}, \tag{4}$$

where $\mathbf{B}(\phi)$ denotes a 16×48 matrix of basis functions:

$$\begin{bmatrix} 1 & \cos(\phi) & \cos(2\phi) & 0 & & \cdots & 0 \\ 0 & 0 & 0 & 1 & \cos(\phi) & \cdots & 0 \\ \vdots & \ddots & & & & & \vdots \\ 0 & \cdots & 1 & \sin(\phi) & \sin(2\phi) & 0 & 0 \\ 0 & \cdots & & 0 & 1 & \sin(\phi) & \sin(2\phi) \end{bmatrix}$$

and the vector $\mathbf{H}$ denotes the harmonic coefficients:

$$\mathbf{H} = [T_{v0}^1, T_{v1}^1, \ldots, T_{V0}^5, T_{V1}^5, T_{V2}^5] \tag{5}$$

Although ideally the polarimetric channels do not contain a zeroth azimuthal harmonic term (see equation (2)), we have included a bias term for the T_U and T_V channels to allow for instrumental measurement errors that can produce such terms. This results in 48 functions of windspeed contained within the vector $\mathbf{H}$.

The harmonic coefficient vector $\mathbf{H}$ is now described in terms of a random function of the wind speed only. Again the brightness temperatures measured by the space-borne radiometer are subject to the influence of the atmosphere and other surface properties as well as instrument noise, but we treat these parameters as nuisance parameters and model their effects on $\mathbf{H}$ probabilistically. The effect of azimuth and polar angle variations across the WindSat swath is also

not explicitly modeled. Specifically we model $\mathbf{H}$ as a multivariate Gaussian random vector with mean vector $\mu_H(W)$ and covariance matrix $\Sigma_H(W)$. The mean vector $\mu_H(W)$ describes the mean harmonic coefficients as a function of windspeed, while the covariance matrix models any errors and correlations among frequency channels or polarizations caused by atmospheric and other effects. Since the effect of the atmosphere on the brightness temperatures is in general a function of the windspeed, the covariance matrix is modeled as a function of the windspeed as well. While the contributions of the atmosphere and surface parameters to measured data may not be perfectly modeled by the Gaussian correlated noise assumption, analytical retrieval performance estimates derived based on the Gaussian assumption are expected to be a conservative estimate for data distributions with the same second order statistics [8] (i.e. with a better fit to the distribution of atmospheric and surface parameter effects on brightnesses.)

The normality assumption of the harmonic coefficients yields the following likelihood function for the brightness temperatures:

$$f(\mathbf{T}|\phi,W) = (2\pi)^{-16/2}|\Sigma_T(\phi,W)|^{-1/2} \quad (6)$$
$$e^{-\left\{0.5(\mathbf{T}-\mu_T(\phi,W))^T\Sigma_T(\phi,W)^{-1}(\mathbf{T}-\mu_T(\phi,W))\right\}},$$

with

$$\mu_T(\phi,W) = \mathbf{B}(\phi)\mu_H(W) \quad (7)$$
$$\Sigma_T(\phi,W) = \mathbf{B}(\phi)\Sigma_H(W)\mathbf{B}^T(\phi). \quad (8)$$

Given estimates of $\mu_T(\phi,W)$ and $\Sigma_T(\phi,W)$, we can form the maximum likelihood estimator (MLE) of wind speed and direction:

$$[\hat{\phi},\hat{W}] = \arg\min_{W,\phi}\big[\ln|\Sigma_T(\phi,W)| + \left\{(\mathbf{T}-\mu_T(\phi,W))^T\Sigma_T(\phi,W)^{-1}(\mathbf{T}-\mu_T(\phi,W))\right\}\big] \quad (9)$$

Use of the MLE requires a two dimensional search over a nonlinear surface in ϕ and W. Typically the log likelihood surface contains multiple local minima leading to possible ambiguities in the wind direction retrieval.

III. Estimation of Model Parameters from WindSat Data

WindSat data release SDR (sensor data record) 1.8.1 contains six months of brightness temperature data from September 2003 to February 2004, as well as collocated data from the QuikSCAT Scatterometer. See [6] for additional information on the WindSat and QuikSCAT collocation procedure. In our parameter estimation step, we used the at-sea data collected over the six month period for which both WindSat and QuikSCAT observations were available (a total of around 56 million observations).

In order to utilize the azimuthal harmonic series of the model, it is required to determine the matrices $\mu_H(W)$ and $\Sigma_H(W)$ from the dataset, and then to find the matrices $\mu_T(\phi,W)$ and $\Sigma_T(\phi,W)$ from $\mu_H(W)$ and $\Sigma_H(W)$ through equations (7) and (8). Because the harmonic coefficients are not directly observed by the radiometer, an iterative approach for estimating $\mu_H(W)$ and $\Sigma_H(W)$ from the available brightness temperatures was developed.

The parameter estimation algorithm first thresholds and discards all data outside the ellipsoid defined by $(\mathbf{T}-\mu)^T\Sigma^{-1}(\mathbf{T}-\mu) \le 40$, where μ and Σ are the empirical mean and covariance of the entire brightness temperature data set. Flagged data points due to aft scan, warm load anomaly, radio frequency interference, land contamination, inland lakes and/or rain [6] are also discarded from the training data. Brightness temperature data is then segmented into wind speed bins of width 1 meters/sec in the interval $[1, 15]$ m/sec to define a dataset $\mathbf{T}_i^W$; here i refers to an index to the points contained within a specific bin. This dataset is further divided into wind direction bins of width 5 degrees resulting in a set of brightness temperatures $\mathbf{T}_i^{\phi,W}$. An iterative least squares (LS) procedure is then applied, as follows:

1) Set $k = 1$; for all wind speed bins, initialize $\Sigma_H^0(W)$ as an identity matrix, and compute $\Sigma_T^0(\phi,W)$ as $\mathbf{B}(\phi)\Sigma_H^0(W)\mathbf{B}(\phi)^T$

2) For each wind speed bin, $\mu_H^k(W)$ is computed using a LS fitting procedure:

$$\mu_H^k(W) = \arg\min_{\mu} \sum_i (\mathbf{T}_i^W - \mathbf{B}(\phi)\mu)^T\left[\Sigma_T^{k-1}(\phi,W)\right]^{-1}(\mathbf{T}_i^W - \mathbf{B}(\phi)\mu)$$

The value of ϕ used in the above is specified by the collocated data; no discretization of ϕ is involved. $\mu_T^k(\phi,W)$ is then found as $\mathbf{B}(\phi)\mu_H^k(W)$.

3) For each bin centered at W and ϕ, compute the sample covariance matrix:

$$S^k(\phi,W) = \frac{1}{N-1}\sum_i (\mathbf{T}_i^{\phi,W} - \mu_T^k(\phi,W))(\mathbf{T}_i^{\phi,W} - \mu_T^k(\phi,W))^T$$

4) For each wind speed bin, a second LS procedure is now used to find

$$\Sigma_H^k(W) = \arg\min_{\Sigma}\sum_{\phi}\|S^k(\phi,W) - B(\phi_i)\Sigma B(\phi_i)^T\|^2$$

$\Sigma_T^k(\phi,W)$ is then computed as $\mathbf{B}(\phi)\Sigma_H^k(W)\mathbf{B}(\phi)^T$

5) Set $k = k+1$ and repeat steps 2-5 until the change in the mean vector μ_H is less than 0.1 %.

The least squares problem in Step 4 seemingly involves the determination of 24 by 49 coefficients, due to the symmetry of the covariance matrix. However the solution for $\Sigma_H(W)$ is not unique, because the brightness temperature observations do not yield an identifiable system of equations for all the correlations between the harmonic coefficients. However, the resulting

covariance matrix estimate $\Sigma_T(\phi, W) = \mathbf{B}(\phi)\Sigma_H^k(W)\mathbf{B}(\phi)^T$ is unique and is the only quantity that is required for ML wind vector estimation. Note the least square fit in Step 4 also is not guaranteed to yield a positive definite covariance matrix $\Sigma_T(\phi, W)$ for every value of ϕ. As a remedy we find the closest positive definite matrix to the estimated $\Sigma_T(\phi, W)$ by raising all eigenvalues which are less than ϵ to ϵ, where ϵ is an estimate for the smallest eigenvalue of the covariance matrix. In this study we used a value of $\epsilon = 0.025$ Kelvin squared. Note due to the small number of parameters to be estimated in this model, it was not deemed necessary to separate the dataset into training and testing subsets, and the entire dataset was utilized in the estimation of μ_H and Σ_H described above. This is reasonable because the number of brightness temperature observations utilized in the parameter estimation procedure vastly exceed the number of parameters to be estimated, so that no "tuning" to a particular brightness observation was involved. Further confirmation was provided by tests using only small training data subsets to estimate model parameters; results showed negligible differences with those obtained using the entire dataset.

Values of $\mu_H(W)$ and $\Sigma_T(\phi, W)$ obtained in this process are discussed further in Section V.

IV. Retrieval Results

We tested the performance of the maximum likelihood windspeed estimator on 130,000 randomly selected brightness temperatures uniformly sampled over the windspeeds of $W \in [2, 14]$ m/sec as reported by QuikSCAT. A scatter plot of retrieved windspeeds versus those obtained from QuikSCAT is provided in Figure 1 (a), which contains all results computed in the study, for all wind direction values. The mean difference (or bias) and root mean square difference between QuikSCAT and retrieved WindSat wind speeds is plotted in Figure 1 (b), together with the results of the EDR 1.8.1 retrieval algorithm for the same set of points. We observe that the two algorithms perform comparably with rms errors in the range 0.7 to 1.2 m/sec that depend weakly on windspeed. The slightly better performance of the ML estimator at high wind speeds is likely due to the fact that ML retrievals were constrained to be in the interval $[1, 15]$ m/sec, while the EDR estimator allows windspeed estimates in excess of 15 m/sec. The bias for both algorithms is very similar, ranges between -0.25 to 0.4 m/sec, and plays a role in the increased rms error at higher wind speeds. Also included in Figure 1 (b) is the analytically estimated rms error (marked "ML predicted"), to be described further in Section VI.

Wind direction retrievals are strongly influenced by ambiguity issues. To illustrate these effects, the likelihood surface for two sample WindSat vectors is displayed in Figure 2: the QuickSCAT data specifies the wind speed and direction for these vectors as $W = 9.8$ m/sec and $\phi = 138.7$ degrees and $W = 6.8$ and $\phi = 202.7$ degrees, respectively. We observe multiple local minima (dark regions in the colored figures) with the global minimum at (9.5 m/sec, 131 deg) and (6.5 m/sec, 287 deg) in each case. One dimensional cuts at the true wind speed and direction given for each case in Figure 3 reveal the local curvature of the likelihood surface which strongly influences the retrieval performance. In the first case, the global minimum value is in agreement with the QuickSCAT wind direction, while the second case illustrates selection of an ambiguity in the wind direction retrieval (i.e. global minimum is not the correct value, while an alternate local minimum yields a better estimation).

Figure 4 (a) is a plot of the difference between wind directions retrieved by the current algorithm and those obtained by QuikSCAT, for a set of 75,000 randomly selected points in the windspeed W interval $[11.5, 12.5]$ m/sec. Evidence of ambiguity selection effects is observed in the results, indicated by the semi-linear trends of the outlier data points. An analysis of these points was performed, and results confirmed that the majority had a minimum in the MLE search closer to the QuickSCAT value. The process was repeated using 10,000 points in each of 13 1 m/s wide wind speed bins centered at $2, 3, \cdots, 14$ m/sec, and Figure 4 (b) plots the resulting rms wind direction differences, along with those achieved by EDR 1.8.1 for the same set of points. RMS differences are plotted both for the first rank (i.e. MLE global minimum value) as well as for the closest (i.e. the MLE local minimum found closest to the QuikSCAT retrieved wind direction) ambiguities. We observe that the proposed algorithm in general displays performance very similar to that achieved by EDR 1.8.1. For the first rank estimates, the MLE algorithm outperforms EDR 1.8.1 by about 5 degrees for wind speeds less than 10 m/sec, while performance is more similar at higher wind speeds. EDR 1.8.1 however produces better closest ambiguity retrievals for windspeeds less than 10 m/sec. This is likely due to the fact that the EDR 1.8.1 retrieval algorithm always records four ambiguities (in some cases based on the global minimum shifted by 90 or 180 degrees), while the current algorithm uses only the number of detected local minima in the likelihood surface, often less than four. Again included in Figure 4 (b) is the analytically predicted rms error (marked 'ML predicted"), to be described further in Section VI. Figure 5 is a plot of the skill (i.e. the percent of time that the first rank ambiguity is the closest ambiguity) for both the current algorithm and for EDR 1.8.1, versus windspeed. The MLE estimate is found to achieve a higher skill for the first rank ambiguity compared to EDR 1.8.1; note EDR 1.8.1 however also has a "selected" ambiguity (skill not shown) that results following a median filtering operation.

To provide a spatial example of the proposed retrieval algorithm, Figure 6 plots wind vectors retrieved on September 14th, 2003 at 10:45 AM UTC in the Caribbean Sea north of Venezuela (region centered at latitude 14N, longitude 71W) using the MLE method (plot a, first rank ambiguities), the first rank retrieval from EDR 1.8.1 (plot b), the selected ambiguity from EDR 1.8.1 (the ambiguity chosen following a median filtering process [5]), and wind vectors from QuikScat (plot d). The QuikScat image shows a relatively smooth wind field with a mean wind speed of 7.7 m/sec and standard variation of 1.3 m/sec. MLE first rank results are very similar to those of the QuikScat image, with a mean retrieved wind speed of 7.4 m/sec and standard deviation of 1.3 m/sec, and show only slight evidence of ambiguity selection issues. Ambiguity

selection issues are more pronounced in the EDR 1.8.1 first rank image, but are reduced following the ambiguity selection process. Overall this example demonstrates that the proposed algorithm can provide reasonable spatial wind field patterns.

While the lesser accuracy achieved by the current algorithm in the closest ambiguity results could likely be mitigated by an inclusion of a larger number of ambiguities in the retrieval process, or else through the application of a spatial filter in post-processing as in the EDR 1.8.1 selected ambiguity, we believe the key result is observed in the first rank ambiguity results, which typically show that the current algorithm is achieving less error than EDR 1.8.1, even though no explicit modeling of the atmosphere is performed. These results suggest that EDR 1.8.1's attempts to model atmospheric effects on wind direction retrievals may be having only minimal impact on overall wind direction retrieval performance. The next section examines the algorithm's operation in greater detail in an attempt to explain these properties.

V. Examination of the retrieval algorithm

In the minimization process of the maximum likelihood estimation (equation (9)) the dominant factor to be minimized is the product

$$\left\{(\mathbf{T}-\mu_T(\phi,W))^T\Sigma_T(\phi,W)^{-1}(\mathbf{T}-\mu_T(\phi,W))\right\} \quad (10)$$

If a diagonalization of $\Sigma_T(\phi,W)^{-1}$ is performed, this product can be interpreted as a sum of the amplitudes (i.e. a result of a vector dot product with itself) of a set of vectors. Each of these vectors is obtained through projection of the the observed brightness vector $\mathbf{T}$ along an eigenvector of $\Sigma_T(\phi,W)^{-1}$, combined with a scaling of this eigenvector by the square root of the associated eigenvalue of $\Sigma_T(\phi,W)$. Since $\Sigma_T(\phi,W)$ is a positive definite matrix, the diagonalization of $\Sigma_T(\phi,W)$ is directly related to that of $\Sigma_T(\phi,W)^{-1}$. This is a standard principal component analysis, and enables some interpretation of the operation of the retrieval algorithm to be obtained.

Note that the $\Sigma_T(W,\phi)$ in this process should be interpreted as the covariance among channels averaged over all environmental conditions with the exception of windvector for the entire six month period. Due to the strong effect of the atmosphere on the linearly polarized channels, it is to be expected that $\Sigma_T(W,\phi)$ will have large entries for cross- or self-covariances involving linearly polarized channels, and smaller entries for cross- or self-covariances involving only polarimetric channels. Analysis of the obtained $\Sigma_T(W,\phi)$ matrices shows this to be true, and also indicates that cross-covariances between linear and polarimetric channels are small.

Due to these properties, the covariance matrix can be well approximated by the block matrix form:

$$\begin{aligned}\Sigma_T(W,\phi) &= \mathbf{B}(\phi)\Sigma_H(W)\mathbf{B}(\phi)^T \\ &\approx \begin{bmatrix} \mathbf{B}^{hv}\Sigma_H^{hv}(\mathbf{B}^{hv})^T & 0 \\ 0 & \mathbf{B}^{UV}\Sigma_H^{UV}(\mathbf{B}^{UV})^T \end{bmatrix} \quad (11)\end{aligned}$$

Use of this block matrix form as opposed to the original $\Sigma_T(W,\phi)$ results in only minor changes in retrieval performance; for example, tests show an wind direction RMS error of 28 degrees for the block matrix form compared to the 26 degrees with the full covariance matrix at windspeed 12 m/sec. This block matrix form is useful in interpreting the algorithm because the block matrix produces separate eigenvectors for the linearly polarized and polarimetric channels.

Tables one and two report components of the principal eigenvectors of $(\Sigma_T^{hv})^{-1}$ and $(\Sigma_T^{UV})^{-1}$ averaged over ϕ and W, listed as T_v, T_h and U, V pairs in the order of increasing frequency. The associated eigenvalues are 1.8 times smaller for the linearly polarized than for the polarimetric eigenvector, showing that the polarimetric channels have less variance, and are therefore emphasized in the retrieval process. This is not surprising given the far larger influence of the atmosphere and other parameters on the linearly polarized channels as discussed previously. The effect of emphasizing the T_U and T_V channels in the likelihood function will be shown in Section VI to influence the dependency of wind direction retrieval accuracy on wind direction. The principal eigenvector of Σ_T^{UV} puts non-trivial weights on the U, V channels at 18.7 GHz as well as the V channels at 10.7 GHz. and 37.0 GHz.

It is interesting to note however that the eigenvalue associated with the linear channels, while smaller than that of the polarimetric channels, remains appreciable, even given the increased atmospheric effects on these channels, so that linear polarizations remain utilized to some degree in the wind direction retrieval process. The principal eigenvector of Σ_T^{hv} shows non-trivial weights on the 10.7, 18.7, and 37.0 GHz channels, and the weights placed on the T_h and T_v channels at each frequency are found generally to have opposite signs with the vertical weight approximately twice that of the horizontal channel in most cases. The channel combination $2T_v - T_h$ has been suggested by other researchers as having a reduced sensitivity to atmospheric parameters. It appears that the estimation procedure attempts to reduced atmospheric effects in a similar manner, although the coefficient multiplying T_v when combined with T_h remains a function of the wind direction, and channels are combined among multiple frequencies as well in the retrieval algorithm.

	6.8	10.7	18.7	23.8	37
T_v	-0.03	0.38	-0.65	0.06	0.39
T_h	-0.05	-0.15	0.32	-0.03	-0.20

TABLE I
COMPONENTS OF THE FIRST EIGENVECTOR OF $(\Sigma_T^{hv})^{-1}$, AVERAGED OVER ϕ AND W

	10.7	18.7	37
U	0.05	-0.18	0.09
V	0.23	-0.54	0.75

TABLE II
COMPONENTS OF THE FIRST EIGENVECTOR OF $(\Sigma_T^{UV})^{-1}$, AVERAGED OVER ϕ AND W

With regard to the estimated mean harmonic coefficients, $\mu_H(W)$, it is clear that atmospheric effects will produce a strong effect on the linearly polarized channels, so that

reasonable harmonic coefficients are very difficult to obtain in the estimation process. In particular, estimation of wind direction variations in these channels is strongly affected by the presence of geophysical correlations between water vapor and wind speed or relative wind direction. The latter is possible because relative wind direction is strongly correlated to absolute wind direction due to the near North-South orientation of the WindSat look direction.

The use of the linearly polarized channels in the retrieval algorithm however can be clarified by examining the azimuthal harmonic coefficients of the composite channel created using the principal eigenvector weighting of the linearly polarized channels at multiple frequencies. Figure 7 is a plot of the composite channel's first and second azimuthal harmonic coefficients as a function of windspeed, and shows typical variations that would be expected for wind direction effects, including small values at low wind speeds. These results indicate that the retrieval algorithm is compensating atmospheric effects reasonably, even though no explicit atmospheric modeling was performed. For completeness, first and second mean harmonic coefficients for the third and fourth Stokes parameters are plotted in Figure 8, and also appear consistent with expectations without any further treatment, due to the greatly reduced influence of the atmosphere on these channels.

VI. Analytical prediction of the proposed wind vector estimator's performance

Maximum likelihood estimators have been widely used in previous wind vector estimation studies [9]. An extensive theory of maximum likelihood estimation is available; it has been shown that such estimators are consistent and asymptotically efficient, *i.e.* the estimate converges to the true value of the parameter for large number of measurements with a mean-square error that can be derived analytically. Here we derive an analytical estimate of the performance of the proposed wind vector estimator, again neglecting any explicit consideration of atmospheric effects. Note that in practice, wind vector estimation typically uses a single measurement at each location, so that the error achieved may be larger than that predicted analytically. Moreover, practical wind vector retrieval algorithms can choose one of the ambiguities (other local minima of the likelihood function), leading to larger errors than the analytical prediction. Even given these issues, analytically predicted error limits provide useful information on the proposed wind vector estimator's expected performance, and allow effects of various system parameters to be examined without repeated empirical MLE retrieval studies.

Let $\mathbf{w} = [W, \phi]$ and $\hat{\mathbf{w}}$ denote the windvector and its unbiased estimator respectively. The Cramer-Rao theorem states that the covariance matrix of the errors is bounded by the inverse of the Fisher Information matrix:

$$E\left[(\mathbf{w}-\hat{\mathbf{w}})^T(\mathbf{w}-\hat{\mathbf{w}})\right] \geq \mathbf{J}^{-1}$$

The Fisher Information Matrix is calculated from the likelihood function as:

$$\mathbf{J} = E\left\{\left[\frac{\partial \ln f(\mathbf{T}|\phi,W)}{\partial \mathbf{w}}\right]\left[\frac{\partial \ln f(\mathbf{T}|\phi,W)}{\partial \mathbf{w}}\right]^T\right\}$$

For the model given in equation (6), the Fisher Information matrix has the following form

$$\mathbf{J} = \begin{bmatrix} \mathbf{J}_{WW} & \mathbf{J}_{W\phi} \\ \mathbf{J}_{\phi W} & \mathbf{J}_{\phi\phi} \end{bmatrix}$$

with

$$\begin{aligned}
\mathbf{J}_{WW} &= \mathbf{A}(W,\phi)\mathbf{B}(\phi)\mu_T'(W) + \frac{1}{2}\mathrm{tr}\left[\mathbf{C}(W,\phi)^2\right] \\
\mathbf{J}_{\phi\phi} &= \mathbf{A}(W,\phi)\mathbf{B}'(\phi)\mu_T(W) + \frac{1}{2}\mathrm{tr}[\mathbf{D}(W,\phi)^2] \\
\mathbf{J}_{W\phi} &= \mathbf{A}(W,\phi)\mathbf{B}'(\phi)\mu_T(W) + \frac{1}{2}\mathrm{tr}\left[\mathbf{D}(W,\phi)\mathbf{C}(W,\phi)\right] \\
\mathbf{J}_{\phi W} &= \mathbf{J}_{W\phi}
\end{aligned}$$

where the prime symbol indicates derivative of a function with respect to its argument, the tr operator indicates the trace of a matrix, and

$$\begin{aligned}
\mathbf{A}(W,\phi) &= \left[\mathbf{B}(\phi)\mu_T'(W)\right]^T \Sigma_T^{-1}(\phi,W) \\
\mathbf{C}(W,\phi) &= \Sigma_T^{-1}(\phi,W)\mathbf{B}(\phi)\Sigma_H'(W)\mathbf{B}(\phi)^T \\
\mathbf{D}(W,\phi) &= \Sigma_T^{-1}(\phi,W)\left[\mathbf{B}'(\phi)\Sigma_H(W)\mathbf{B}(\phi)^T\right. \\
&\quad \left. + \mathbf{B}(\phi)\Sigma_H(W)\mathbf{B}'(\phi)^T\right] \qquad (12)
\end{aligned}$$

In particular the mean square errors of the wind speed and the wind vector estimates are bounded by:

$$E\left[(W-\hat{W})^2\right] \geq \left(\mathbf{J}_{WW} - \frac{\mathbf{J}_{W\phi}^2}{\mathbf{J}_{\phi\phi}}\right)^{-1} \qquad (13)$$

$$E\left[(\phi-\hat{\phi})^2\right] \geq \left(\mathbf{J}_{\phi\phi} - \frac{\mathbf{J}_{W\phi}^2}{\mathbf{J}_{WW}}\right)^{-1} \qquad (14)$$

The form of the error bounds obtained above clearly depends on both wind speed and direction for both the wind speed and direction estimators. These variations are examined in detail in the next section.

VII. Results of analytical performance predictions

Given the obtained values of the mean vector $\mu_T(\phi, W)$ and the covariance matrix $\Sigma_T(\phi, W)$, analytical error estimates are evaluated from equations (13) and (14). In order to calculate the required derivatives $\mu_H'(W)$, a cubic polynomial is fit to the harmonic coefficients. The contribution of $\Sigma_H'(W)$ is found to be negligible compared to the other terms.

Figure 9 illustrates analytically predicted errors in wind speed estimation as a function of the wind speed for $\phi = 0, 45, ..., 180$ degrees. The wind speed estimation performance is observed to be relatively insensitive to windspeed, with a root mean square error ranging from 0.7 to 1.4 meters/sec over the range of wind speeds considered. The wind speed estimator performance shows only a weak dependence on the wind direction ϕ. Note the similar wind speed estimation performance obtained at $\phi = 0$ and $\phi = 180$ degrees compared to other wind directions shows that information from the horizontally and vertically polarized channels is being utilized

in the retrieval process, as discussed in Section V, since the polarimetric channels contain no wind speed information at these angles. An average of these curves over wind direction was included in Figure 1 (b).

Figure 10 plots predicted wind direction estimation errors for the proposed model as a function of wind speed and direction. We observe that with increasing wind speed the accuracy of the wind direction estimates improves, to within approximately 10 degrees at all wind directions for $W = 13$ m/sec. We also observe that the wind direction estimator performance is not uniform over the set of relative wind directions. A similar curve averaged over wind direction is included in Figure 4 (b) versus windspeed, and shows that the predicted estimator performance is reasonably close to that achieved by the closest ambiguity in the empirical MLE wind direction retrieval. The first rank empirically-obtained error approaches the predicted value only at higher windspeeds, presumably due to a reduction in ambiguity selection errors as the wind direction influence on brightnesses increases.

To assist in interpreting the predicted wind direction estimation errors and their dependence on wind direction, a simple model of wind direction estimation from the T_U and T_V channels at a single frequency can be used. Specifically we consider the model:

$$T_U = a_1 \sin(\phi) + a_2 \sin(2\phi) + n_U$$
$$T_V = b_1 \sin(\phi) + b_2 \sin(2\phi) + n_V$$

Here the coefficients a_1, a_2, b_1, b_2 are assumed to be fixed and known parameters, while n_U, n_V are Gaussian zero mean uncorrelated random noise with known variance σ^2. The analytically predicted error for this simple model is given by:

$$E\left[(\phi - \hat{\phi})^2\right] \leq \sigma^2 \left((a_1 \cos(\phi) + 2a_2 \cos(2\phi))^2 + (b_1 \cos(\phi) + 2b_2 \cos(2\phi))^2\right)^{-1}$$

Figure 11 plots these predicted errors for $a_1 = 1.0$, $a_2 = -0.7$, $b_1 = -0.1$, $b_2 = 5$, and $\sigma = 0.1$ (all in Kelvin); these values are somewhat similar to those observed in Figure 8 at 18.7 GHz near $W = 13$ m/sec. We observe that this simple model appears to capture many of the features of the results in Figure 10 for the complete model of WindSat data.

Because predicted errors have been shown to match reasonably those obtained in empirical MLE retrievals, analytical predictions can be utilized to examine other retrieval processes. As an example, the effect of excluding various channels in the proposed model for wind vector estimation was studied. The results reveal that any two of the three fully polarimetric frequency bands provide competitive wind vector estimation performance. Figure 12 for example illustrates predicted errors for a system using only the 10.7 and 37 GHz channels; windspeed retrieval accuracy is degraded only slightly while wind direction estimation shows larger variations in the errors versus wind direction along with only slightly increased mean errors.

VIII. Conclusions and Future Work

This paper has presented a simple stochastic model that relates WindSat measured brightness temperatures to windspeed and direction, under the assumption that atmospheric and environmental effects other than windspeed need not be explicitly modeled. The required mean and covariance matrices of the model were evaluated using a subset of co-located WindSat and QuickSCAT measurements. The stochastic model yielded a maximum likelihood estimator for wind vector parameters; we characterized the retrieval performance of this maximum likelihood estimator and showed overall first-rank ambiguity errors compared to QuickSCAT wind vectors comparable to those achieved by WindSat EDR 1.8.1. Closest ambiguity errors were larger than those of WindSAT EDR 1.8.1, but the larger number of EDR 1.8.1 ambiguities retained likely contributes to this difference. An analysis was performed to show that the proposed model still attempted to remove atmospheric effects in the linearly polarized channels through a weighting similar to the $2T_v - T_h$ algorithm recommended by other investigators. Analytical predictions of the proposed algorithm's retrieval performance were also explored, and showed in general that wind direction retrieval errors should be expected to depend on the relative wind direction as well as the wind speed.

Future work will extend the comparison to include the more recent EDR 1.9.0, as well as consider generalizing the model to make the effect of atmospheric and environmental parameters explicit, by modeling the harmonic coefficients as functions of windspeed as well as column water vapor (V), cloud liquid water (L), and surface temperature (T_S). It is interesting to note however that the retrievals obtained here showed reasonable wind speed and wind direction estimation performance while such effects were neglected. Nevertheless, generalization to include these effects would likely be especially valuable in the analysis of brightness temperatures over multiple pixels, because the effects of V,L, and T_S on the brightness temperatures are likely to be spatially correlated. Such an approach could potentially reduce remaining ambiguity problems in wind direction estimation.

References

[1] P. W. Gaiser, K. St. Germain, E. M. Twarog, G. A. Poe, W. Purdy, D. Richardson, W. Grossman, W. L. Jones, D. Spencer, G. Golba, M. Mook, J. Cleveland, L. Choy, R. M. Bevilacqua, and P. Chang, "The WindSat space borne polarimetric microwave radiometer: sensor description and early orbit performance," *IEEE Trans. Geosci. Remote Sensing*, vol. 42, no. 11, Nov 2004.

[2] P. W. Gaiser and e. C. S. Ruf, "Windsat special issue," *IEEE Transactions on Geoscience and Remote Sensing*, vol. 44, no. 3, March 2006.

[3] F. J. Wentz, "Measurement of oceanic wind vector using satellite microwave rradiometers," *IEEE Trans. Geosci. Remote Sensing*, vol. 33, no. 5, Sep 1992.

[4] S. H. Yueh, W. J. Wilson, S. J. DiNardo, and F. K. Li, "Polarimetric microwave brightness signatures of ocean wind direction," *IEEE Trans. Geosci. Remote Sensing*, vol. 37, no. 2, Mar 1999.

[5] M. H. Bettenhausen, C. K. Smith, R. M. Bevilacqua, N. Wang, P. W. Gaiser, and S. Cox, "A nonlinear optimization algorithm for windsat wind vector retrievals," *IEEE Transactions on Geoscience and Remote Sensing*, vol. 44, no. 3, pp. 567–610, March 2006.

[6] Physical Oceanography Distributed Active Archive Center, "http://podaac.jpl.nasa.gov/ windsat," March 2005.

[7] S. H. Yueh, R. Kwok, and S. V. Nghiem, "Polarimetric scattering and emission properties of targets with reflection symmetry," *Radio Sci.*, vol. 29, Nov 1994.

[8] P. Stoica and R. L. Moses, *Introduction to Spectral Analysis*. Prentice Hall, 1997.

[9] C. Y. Chi and F. K. Li, "A comparative study of several wind estimation algorithms for spaceborne scatterometers," *IEEE Trans. Geosci. Remote Sensing*, vol. 26, no. 2, Mar 1988.

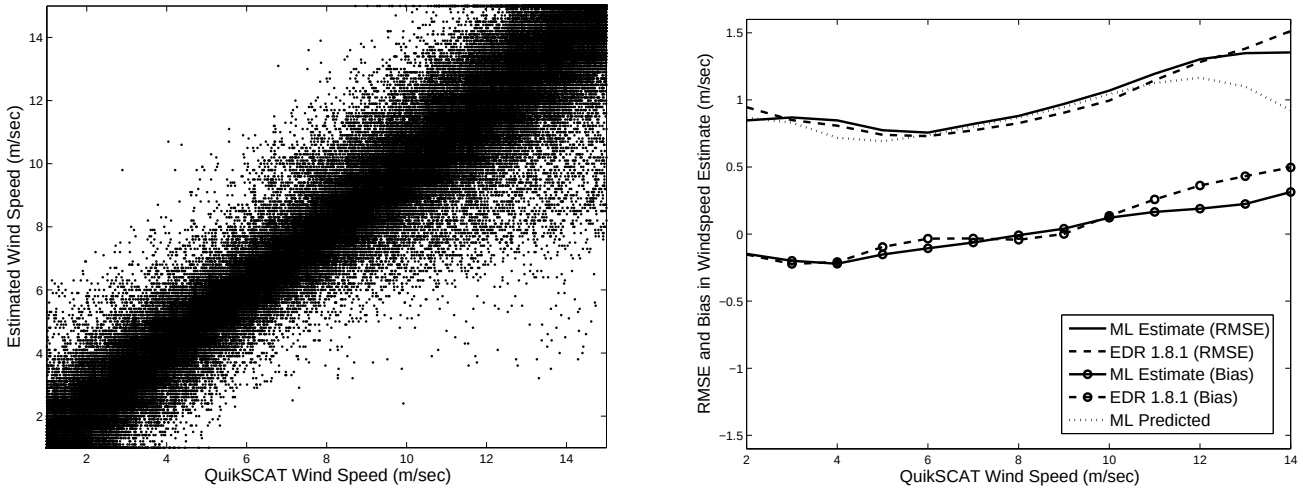

(a) Scatter Plot

(b) RMSE Performance

Fig. 1. Windspeed estimation performance of the MLE

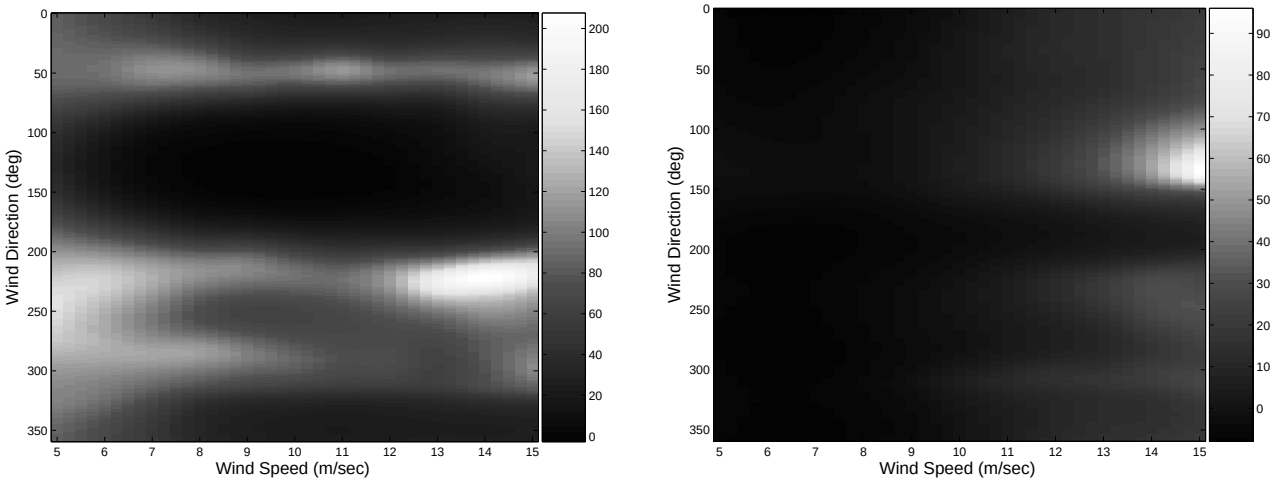

(a) $W = 9.8$ m/sec and $\phi = 138.7$

(b) $W = 6.8$ m/sec and $\phi = 202.7$

Fig. 2. Likelihood Surfaces for two sample WindSat vectors

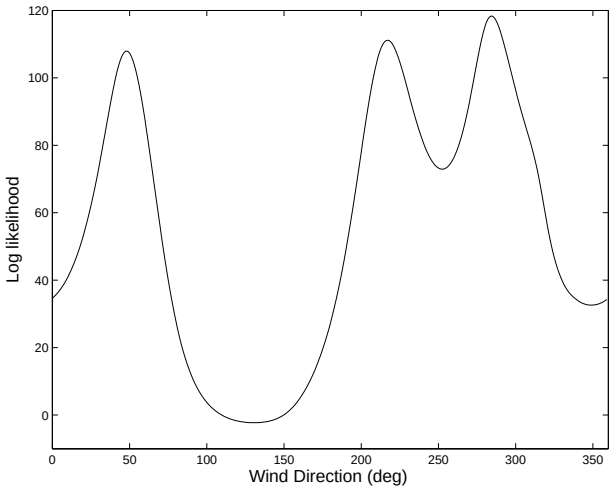

(a) $L(\phi, \cdot)$ for $\mathbf{w} = (9.8$ m/sec, 139 degrees)

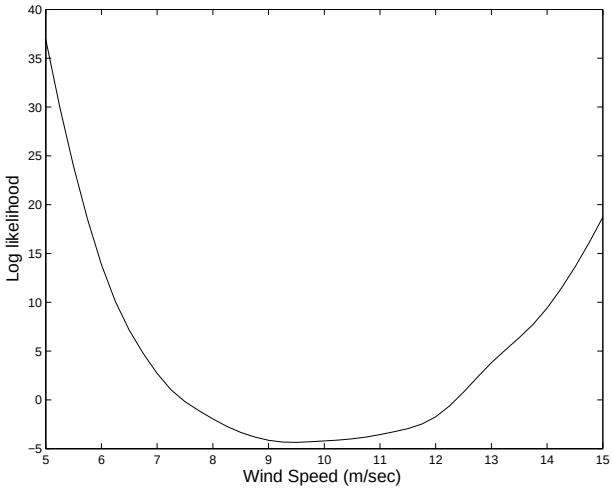

(b) $L(\cdot, W)$ for for $\mathbf{w} = (9.8$ m/sec, 139 degrees)

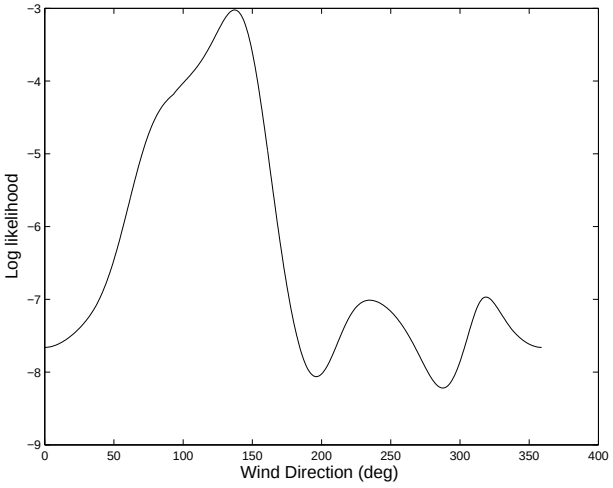

(c) $L(\phi, \cdot)$ for for $\mathbf{w} = (6.8$ m/sec, 203 degrees)

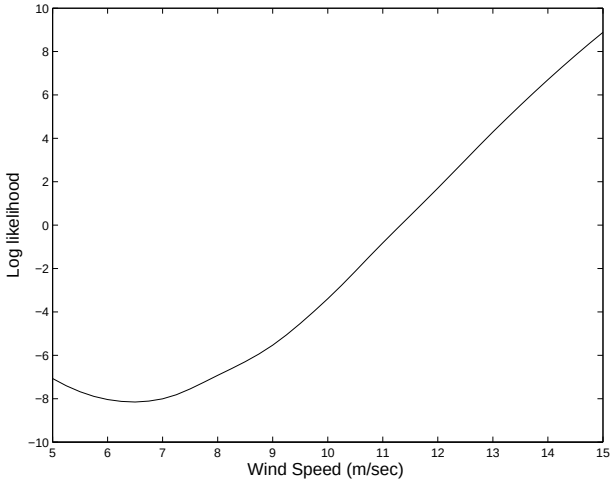

(d) $L(\cdot, W)$ for $\mathbf{w} = (6.8$ m/sec, 203 degrees)

Fig. 3. One dimensional cuts of the Likelihood Surface $L(\phi, W)$

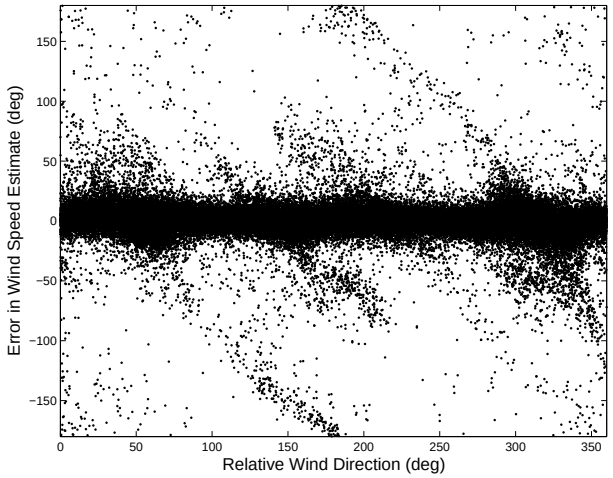

(a) Scatter Plot for $W = 12$ m/sec

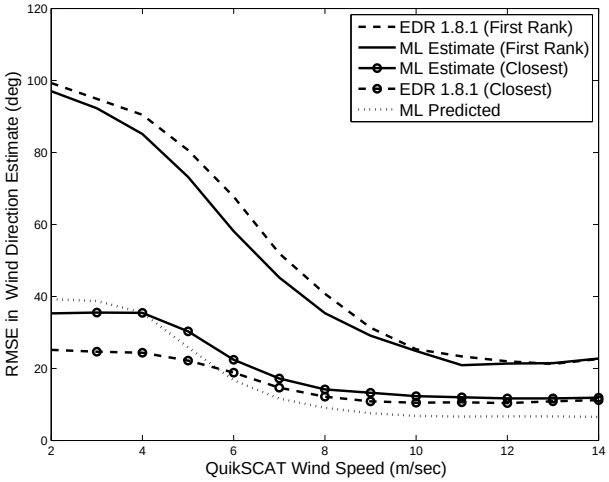

(b) RMSE Performance as a function of W

Fig. 4. Wind-direction estimation performance of the MLE

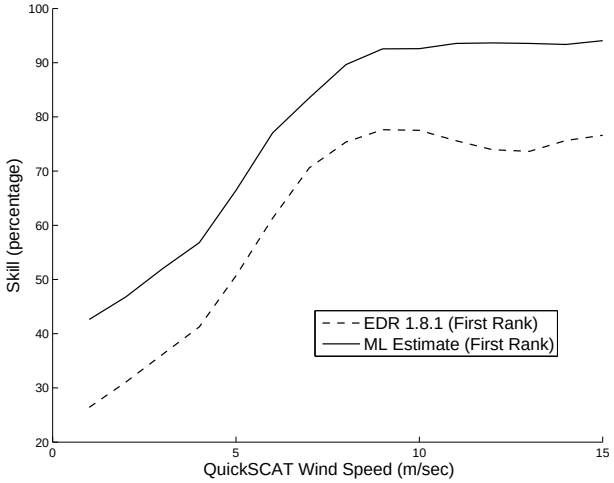

Fig. 5. Ambiguity selection skill (for first rank ambiguities) of the MLE and EDR 1.8.1 versus windspeed

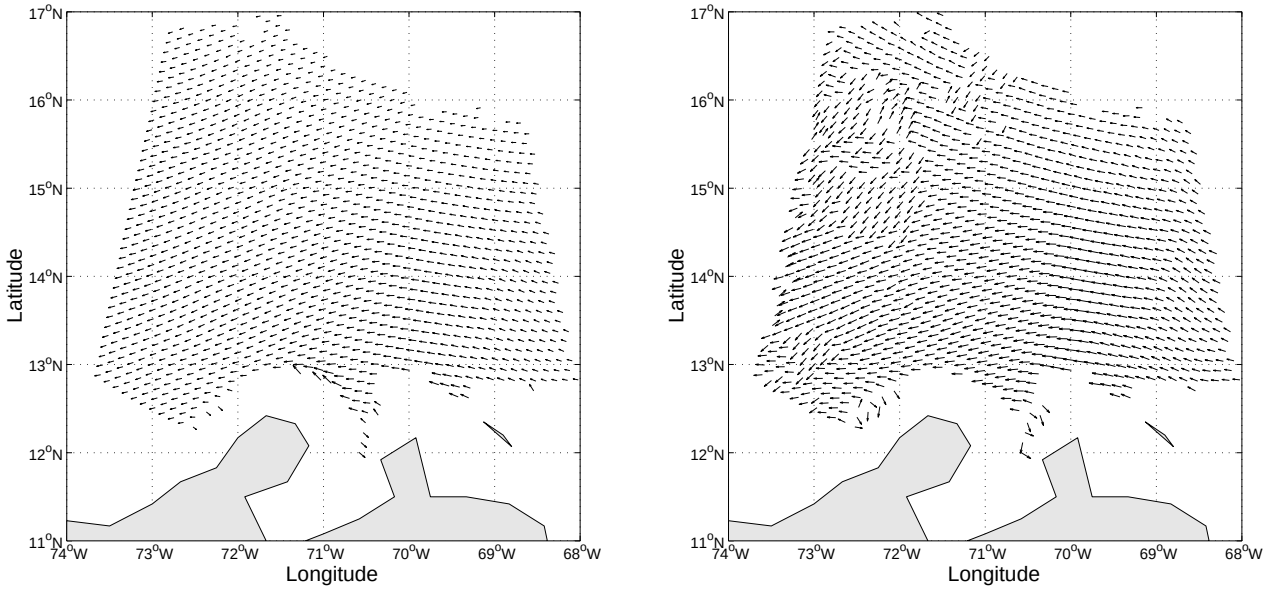

(a) Proposed Estimator

(b) EDR 1.8.1 (First Rank)

(c) EDR 1.8.1 (Selected)

(d) QuikSCAT

Fig. 6. Ocean wind vector retrievals for September 14, 2003 at 10:45am UTC in the Caribbean sea (a) First rank retrieval from MLE technique (b) EDR 1.8.1 first rank retrieval (c) EDR 1.8.1 selected ambiguity retrieval (d) QuikScat wind vectors

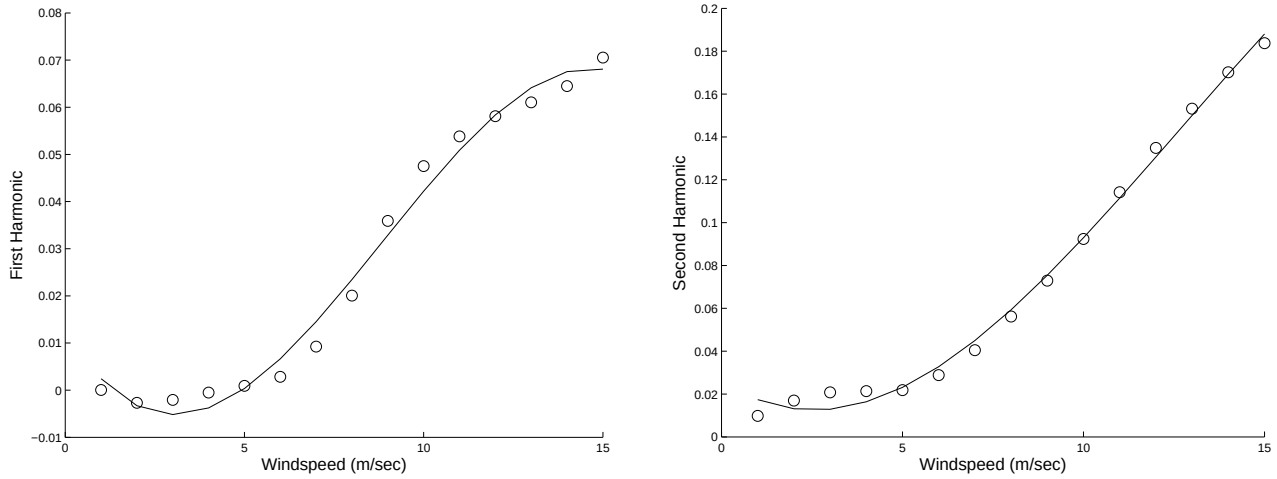

(a) First Harmonic Coeffi cient

(b) Second Harmonic Coeffi cient

Fig. 7. First and Second Harmonic of the wind direction retrieved from the linear combination of T_h and T_v polarizations, as a function of windspeed. Solid curves are a polynomial fi t to the obtained data (symbols).

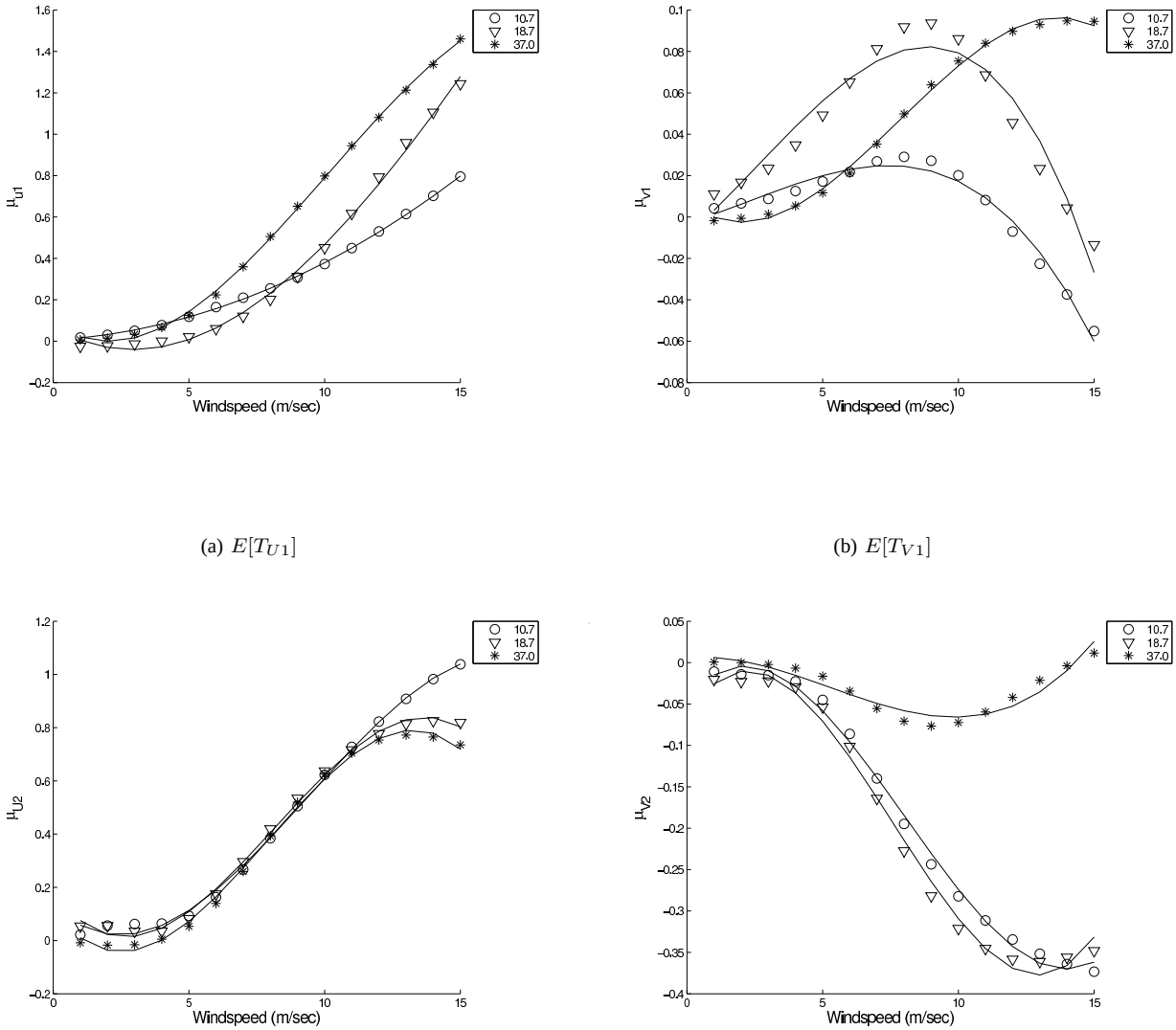

(a) $E[T_{U1}]$

(b) $E[T_{V1}]$

(c) $E[T_{U2}]$

(d) $E[T_{V2}]$

Fig. 8. Elements of the model function parameter vector μ_H in T_U and T_V polarizations, as a function of windspeed. Solid curves are a polynomial fit to the obtained data (symbols).

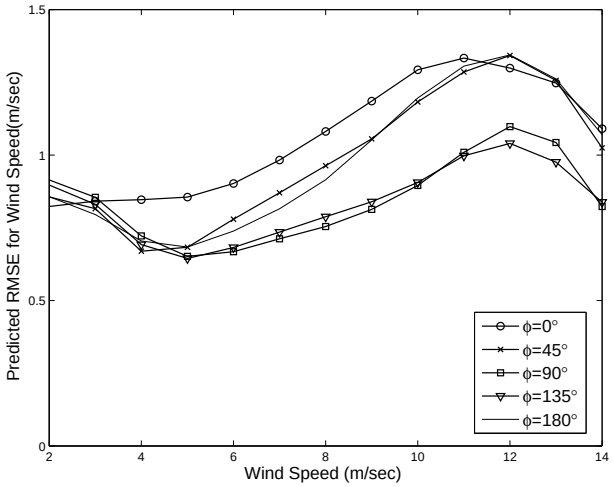

Fig. 9. Predicted errors in wind speed estimation for proposed algorithm, for $\phi = 0, 45, 90, 135$ and 180 degrees

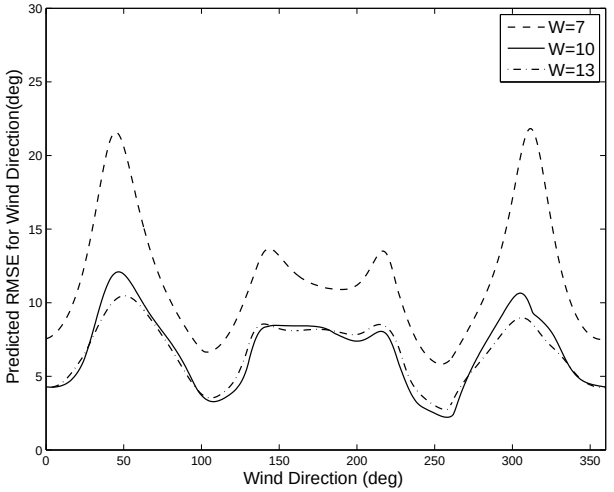

Fig. 10. Predicted errors in wind direction estimation for proposed algorithm, at $W = 7, 10$, and 13 m/sec

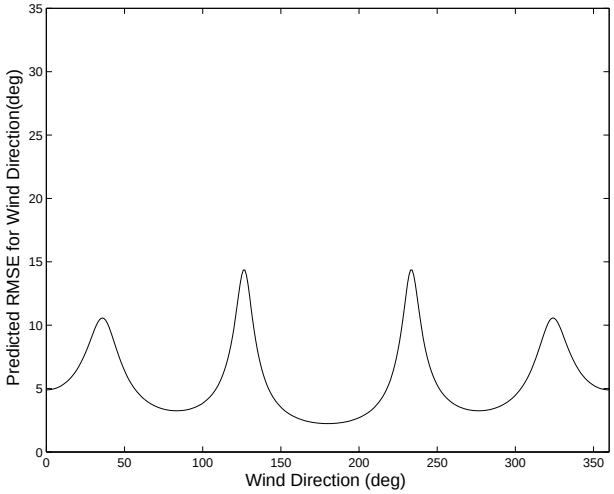

Fig. 11. Predicted errors in wind direction estimation for a simple model of T_U and T_V channels at a single frequency band

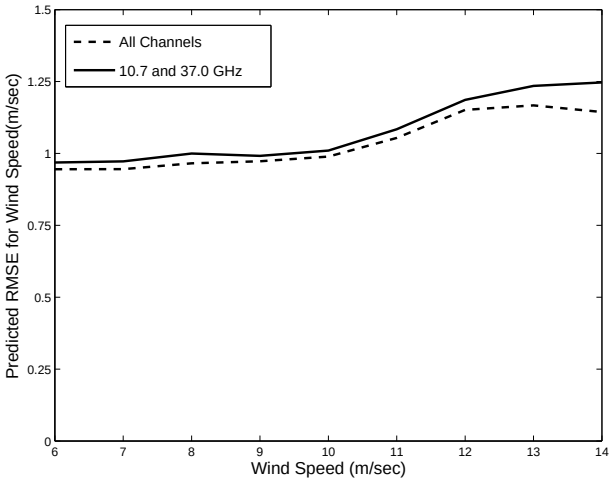

(a) Predicted errors in wind speed estimation for $\phi = 0$ deg

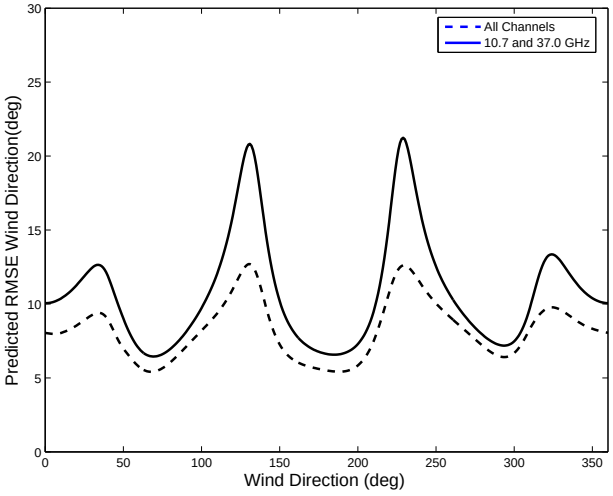

(b) Predicted errors in wind direction estimation for $W = 12$ m/sec

Fig. 12. Wind-vector estimation performance with 10.7 and 37 GHz Channels